Article

Monitoring Within-Field Variability of Corn Yield using Sentinel-2 and Machine Learning Techniques

Ahmed Kayad [1,2,*] , **Marco Sozzi** [1] , **Simone Gatto** [3] , **Francesco Marinello** [1] and **Francesco Pirotti** [1]

[1] Department TESAF, University of Padova, viale dell'Università 16, 35020 Legnaro (PD), Italy; marco.sozzi@phd.unipd.it (M.S.); francesco.marinello@unipd.it (F.M.); francesco.pirotti@unipd.it (F.P.)
[2] Agricultural Engineering Research Institute (AEnRI), Agricultural Research Centre, Giza 12619, Egypt
[3] Porto Felloni srl, 44023 Lagosanto (FE), Italy; simo9cat@libero.it
[*] Correspondence: ahmed.kayad@phd.unipd.it

check for updates

Abstract: Monitoring and prediction of within-field crop variability can support farmers to make the right decisions in different situations. The current advances in remote sensing and the availability of high resolution, high frequency, and free Sentinel-2 images improve the implementation of Precision Agriculture (PA) for a wider range of farmers. This study investigated the possibility of using vegetation indices (VIs) derived from Sentinel-2 images and machine learning techniques to assess corn (*Zea mays*) grain yield spatial variability within the field scale. A 22-ha study field in North Italy was monitored between 2016 and 2018; corn yield was measured and recorded by a grain yield monitor mounted on the harvester machine recording more than 20,000 georeferenced yield observation points from the study field for each season. VIs from a total of 34 Sentinel-2 images at different crop ages were analyzed for correlation with the measured yield observations. Multiple regression and two different machine learning approaches were also tested to model corn grain yield. The three main results were the following: (i) the Green Normalized Difference Vegetation Index (GNDVI) provided the highest R^2 value of 0.48 for monitoring within-field variability of corn grain yield; (ii) the most suitable period for corn yield monitoring was a crop age between 105 and 135 days from the planting date (R4–R6); (iii) Random Forests was the most accurate machine learning approach for predicting within-field variability of corn yield, with an R^2 value of almost 0.6 over an independent validation set of half of the total observations. Based on the results, within-field variability of corn yield for previous seasons could be investigated from archived Sentinel-2 data with GNDVI at crop stage (R4–R6).

Keywords: Sentinel-2; precision agriculture; machine learning; vegetation indices; corn yield; within-field variability; digital farming

1. Introduction

Crop yield is defined as the total production per unit area and is commonly measured in tons per hectare [1]. Such yield changes spatially and temporally within-field zones based on local spatial variability in soil physical and chemical properties, management practices and localized damage due to pests and pathogens [2–4]. Information on within-field yield variability supports farmers to improve their management decisions, profit, land rental, and for insurance assessment as well [5,6]. The first step in PA is yield monitoring, which is one of the fundamental elements for delineating management zones (MZ) based on previous yield maps [7]. Delineating MZ requires information on soil characteristics and archived management practices for the field, while yield monitoring evaluates the final result of these practices at the end of the growing season.

Satellite remote sensing (RS) offers a wide range of indications for crop and vegetation parameters, such as Leaf Area Index (LAI) [8,9], leaf nitrogen accumulation [10], the fraction of absorbed photosynthetically active radiation (FPAR) [11] and crop biomass [8,12–14]. Most of these applications were on the large scale of a region or country compared with few applications at a field scale. The most common reasons for this trend are the high cost of obtaining and processing RS data on a field scale, research funders such as governments and organizations are focusing on total production, and a lack of ground truth data and measurement accuracy [5].

Traditional methods for crop yield monitoring such as quadratic frame sampling are time-consuming, destructive, laborious, and not accurate for large fields where spatial variability becomes an issue [2]. Currently, the availability of crop yield monitoring systems mounted to harvesters can provide yield maps but obviously only at the end of the season. Therefore, the rapid development in RS and the need for crop yield monitoring and prediction attracts the attention of many researchers to investigate within-field variability through satellite and aerial RS data [15–19].

In most yield monitoring studies using RS data, two main strategies have been typically proposed. The first method integrates RS data with meteorological data and plant physiological models to monitor crop development and then crop yield [20,21]. The other method relies on RS data to predict the yield for crops that have a direct relation between biomass and the harvest index [22]. The harvest index is the ratio between grain yield and above ground crop biomass. The first method is complicated and requires a lot of inputs, while the latter method does not provide an explanation of physiological process [23].

The development of empirical equations between vegetation indices (VIs) and crop yield is a simple and operational way to assess within-field variability [24,25], whereas the developed equations have spatial and temporal constraints to apply in another field or another season [19,26,27]. A large number of VIs have been developed to describe crop growth and subsequently yield. Some well-known ones are the Normalized Difference Vegetation Index (NDVI), Soil Adjusted Vegetation Index (SAVI), Enhanced Vegetation Index (EVI), Green Normalized Difference Vegetation Index (GNDVI), Green Atmospherically Resistant Vegetation Index (GARVI), and Normalized Difference red edge (NDRE) [16,28–32]. Specific modifications by differential weighting of some bands (in particular of the near-infrared range) have been applied to provide specific indices for crop yield monitoring, like the Wide Dynamic Range Vegetation Index (WDRVI) [33,34] and the Green Chlorophyll Vegetation Index (GCVI) [35]. Selecting the most suitable VI and crop age for yield assessment is an important step in crop yield empirical model development [16].

Predicting corn (*Zea mays* L.) grain yield and assessing its spatial and temporal variability have been investigated in several studies [24,26,36–40]. Lobell et al. [5] introduced a yield prediction method based on Landsat 5 and Landsat 7 satellite imagery and weather data used as inputs with crop model simulations. This approach was tested between different fields based on farmers reports in the USA and the overall R^2 for corn was 0.35. Shanahan et al. [41] reported that GNDVI derived from aircraft imagery at mid-grain filling stage provided the highest correlations (0.7 to 0.92) with corn grain yield in a plots experiment. Bognar et al. [42] used the greenness index derived from the Advanced Very High Resolution Radiometer (AVHRR) imagery to predict corn yield at the Hungarian county scale with 90% accuracy in late July (70 days before harvesting). A recent study was performed in Brazil and the USA to investigate different VIs derived from Sentinel-2 images to predict corn grain yield at a field scale. The collected images were in the range of ±20 days from flowering. This study showed that NDRE, GNDVI, and NDVI presented high performance to forecast field variability and provided an R^2 value of 0.32 for the universal corn yield estimation equation [19].

Currently, various agricultural models based on RS imagery have been developed using Machine Learning (ML) techniques [43–45]. ML techniques potentially provide a higher accuracy and a more robust performance compared to conventional correlations as they learn to model complexity through training. Therefore, variance is explained through either parametric or nonparametric approaches. Parametric approaches are simpler, need less data for training, but are less suited for complex problems.

Nonparametric models are harder to interpret with regards to input features, need more time and more data for training, and can suffer from overfitting, but by making no assumptions in the underlying function, they are more flexible [46].

A note must be made about deep learning methods. Applications of deep learning to imagery in the literature have proven to give added accuracy and improve results. In this study, deep learning methods were not considered because of the implicit complexity to the deep learning approach. The complexity lies in defining the architecture of the hidden layers that require testing combinations of pooling layers and convolutional layers with the respective parameters. The ML methods tested in this investigation only require tuning a few parameters. It is certainly worth testing deep learning methods, but this was not the focus of this research.

In this work we tested three regression methods. One is a common multiple linear Regression (MR), and two are ML algorithms, Random Forests (RF) and Support Vector Machines (SVM). The two ML approaches are more effective as they are not affected by collinearity and non-normal distribution of the variables, can handle overfitting, and do not require scale normalization. They are nonparametric models, as opposed to MR, and therefore have the drawback that they add complexity to interpretation. Recently, ML algorithms have emerged with big data technologies to create new opportunities in the agricultural domain [47]. Applying ML algorithms on crop yield estimation from RS data is a flexible approach and capable of processing a large number of inputs with the increase in data volumes due to higher resolution and the shorter revisit times of new satellite sensors [48].

Yuan et al. [45], compared different ML techniques to estimate the LAI of soybean using Unmanned Aerial Vehicle (UAV) imagery and reported that RF was the most suitable technique when the sample plots and variations in LAI were relatively large. Yue et al. [49] reported that RF was extremely robust against noise compared with other ML techniques in estimating winter wheat biomass using near-surface spectroscopy. Karimi et al. [50] used SVM and Artificial Neural Networks (ANN) to classify hyperspectral images based on nitrogen application rates and weed management practices over a corn field and the results showed that SVM provided very low misclassification rates compared with ANN. In addition, they recommended the SVM technique for early stress detection in corn, which could aid in effective early application of site-specific remedies. Han et al. [51] applied MR, ANN, SVM, and RF algorithms on UAV RS data to predict the above ground maize biomass and their results showed that RF provided the most balanced results with low error.

Monitoring within-field variability requires sufficient spatial and temporal resolutions according to crop type and targeted application [6,18]. In the case of corn, which represents about 20% of Italian cereal cultivated area, more than 80% of corn fields have an area over 10 ha [52]. The Sentinel-2 satellite constellation provides images with a 10 m spatial resolution for red, green, blue, and near-infrared (NIR) bands, which is equivalent to 1000 pixels in a 10 ha field. Moreover, the corn growing seasons are spring and summer (April to September), which have fewer clouds compared to other seasons, and Sentinel-2 provides images with a 5-day revisit frequency [53]. Thus, Sentinel-2 provides images that have sufficient spatial and temporal resolutions for monitoring within-field variability in Italian corn fields.

The purpose of this paper was to evaluate the potential of using different VIs derived from archived Sentinel-2 satellite images for identifying corn yield spatial variability within-field and compare results with three regression methods that have been proven to perform best in the recent literature: random forests (RF), support vector machines (SVM), and multiple regression (MR). The specific objectives were

(1) to examine different vegetation indices for corn yield estimation;
(2) to define the suitable crop age for predicting yield variability within the field scale;
(3) to develop a corn yield prediction model based on Sentinel-2 images and the best performing machine learning technique and compare the results with VIs.

2. Materials and Methods

2.1. Study Area

This study was carried out on a 22-ha field located in a typical valley area (at Porto Felloni Co.) in Ferrara, North Italy (Figure 1). The study field lies within the Mediterranean climatic zone and the total rainfall during the corn growing season was 266 mm on average. The soil texture is silt loam and the study field has been irrigated by a center pivot irrigation system and cultivated with corn for two decades, with the exception of 2015, when it was cultivated with wheat. This work focused on three years of corn cultivation from 2016 to 2018. The corn planting dates were 30 March 2016, 22 March 2017 and 11 April 2018 for the study field and harvest was done at a crop age of 160 days on average. The company cultivated the same corn seed variety (Pioneer P1916) during the study period with 75 cm of row spaces and 16 cm between seeds, on average. Additionally, they used a variable rate of nitrogen application with an average urea application (nitrogen 46%) of 344 kg/ha in 2016 and 2017 and 367 kg/ha in 2018. The prescription map of applied nitrogen was the same for the 2016 and 2017 seasons and modified for the 2018 season.
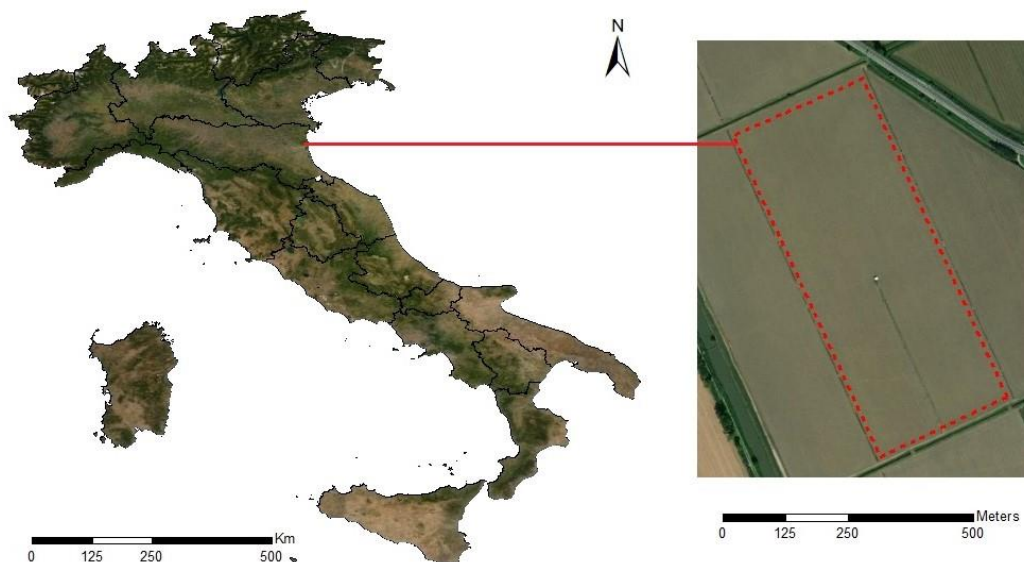
Figure 1. Study field in Ferrara, North Italy.

2.2. Measured Yield Data

A grain yield monitoring system mounted on a combine harvester was used to record corn yield. This system could record about 1000 yield points for each hectare (about 20,000 points from the whole study field). The harvester width was 6 m and the monitor could record yield every 1 s, which is equivalent to an average speed of the harvester of 1.5 m along the direction of harvesting. Corn yield varied between 9 and 18 ton/ha across the study field for the three seasons. After harvesting and downloading the yield data, maps were processed as follows. Field borders were removed to avoid noise arising from the partial presence of corn in the field margins. Data recorded while the harvesting machine was turning at the end of each line were also removed to avoid zero production from the corresponding field portions. Secondly, two lines were removed from the 2016 yield data where the harvester passed twice during field operations. The measured yield is provided as a dataset with ~20,000 sparse points, whereas the Sentinel-2 data is a raster with a 10-m resolution. Therefore, the sparse points were interpolated to a raster with the same resolution as Sentinel-2 using the Kriging method. Kriging was run using R's Gstat package. The best models and fits (range, partial sill, and nugget) are, respectively, for each of the three seasons from 2016 to 2018: (i) Exponential—57.29 m, 1.628, 2.78; (ii) Exponential—46.18 m, 3.087, 5.123; (iii) Spherica—114.87 m, 3.982, 5.55. The field contains

2006 cells with yield values for each of the three seasons analyzed. Figure 2 shows a color-scaled image of the final corn yield data for the three studied seasons.
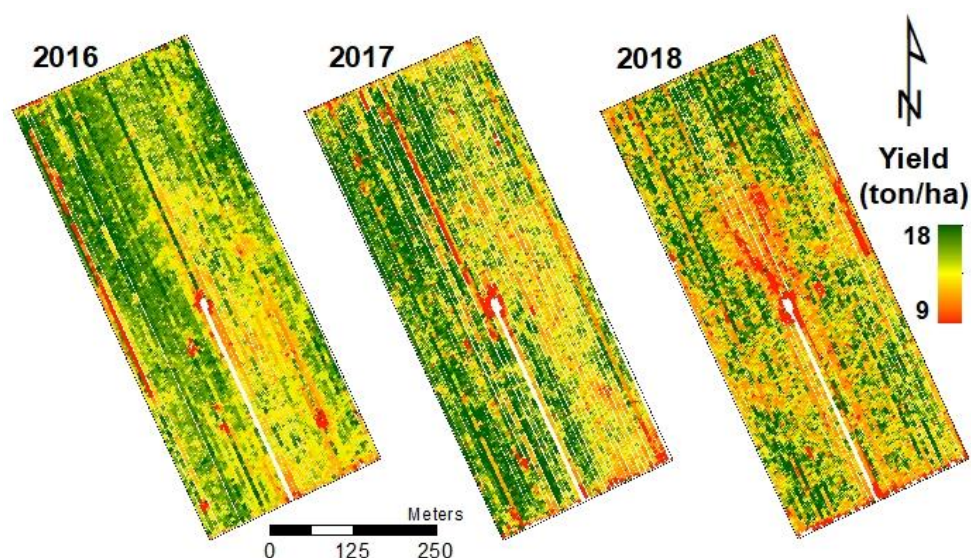
Figure 2. Corn grain yield data for the 2016, 2017, and 2018 growing seasons.

2.3. Satellite Imagery

Sentinel-2 Level 2A (L2A) Bottom-Of-Atmosphere (BOA) reflectance product was acquired from the Copernicus Open Access Hub. Sentinel-2 L2A data provided 12 bands with channels ranging from 443 to 2190 nm and a spatial resolution (ground sampling distance—GSD) of 10 to 60 m [54]. All images were resampled to 10 m pixel size and clipped to the region of interest (the study field).

To compare between the plant development stages, we used "crop age", defined by the number of days counted from the planting date. The crop ages at harvesting time were 168, 159, and 160 days from planting for 2016, 2017, and 2018, respectively. In our case, there were no available cloud-free Sentinel-2 images until a crop age of 60 days (April and May). Starting from June, cloud-free satellite images were more frequently available. In 2016, there were only six Sentinel-2 images available. This number increased to reach 14 images per season for 2017 and 2018. A total of 34 Sentinel-2 images between 2016 and 2018 were available during the corn growing season at different crop ages, as shown in Table 1.

Table 1. Sentinel-2 images dates corresponding crop age in days and phenological stage at each growing season.

2016 Season			2017 Season			2018 Season		
Planting Date: 30 March 2016 Harvesting Date: 14 September 2016			Planting Date: 22 March 2017 Harvesting Date: 25 August 2017			Planting Date: 11 April 2018 Harvesting Date: 18 September 2018		
I	**Date**	**Age (Stage)**	**I**	**Date**	**Age (Stage)**	**I**	**Date**	**Age (Stage)**
1	18 June 2016	80 (R3)	1	31 May 2017	70 (R2)	1	19 May 2018	38 (V10)
2	18 July 2016	110 (R4)	2	03 June 2017	73 (R2)	2	10 June 2018	60 (R1)
3	28 July 2016	120 (R5)	3	13 June 2017	83 (R3)	3	15 July 2018	95 (R3)
4	04 August 2016	127 (R6)	4	20 June 2017	90 (R3)	4	18 July 2018	98 (R4)
5	14 August 2016	137 (R6)	5	23 June 2017	93 (R3)	5	20 July 2018	100 (R4)
6	24 August 2016	147 (R6)	6	03 July 2017	103 (R4)	6	28 July 2018	108 (R4)
			7	10 July 2017	110 (R4)	7	04 August 2018	115 (R6)
			8	13 July 2017	113 (R5)	8	17 August 2018	128 (R6)
			9	23 July 2017	123 (R6)	9	19 August 2018	130 (R6)
			10	30 July 2017	130 (R6)	10	22 August 2018	133 (R6)
			11	02 August 2017	133 (R6)	11	24 August 2018	135 (R6)
			12	04 August 2017	135 (R6)	12	27 August 2018	138 (R6)
			13	12 August 2017	143 (R6)	13	29 August 2018	140 (R6)
			14	22 August 2017	153 (R6)	14	06 September 2018	148 (R6)

Clouds and other opaque aerosol in the atmosphere can partially occlude the transmission of energy at the wavelengths recorded by the Multispectral Instrument (MSI) on-board Sentinel-2. Level 2A products provide a raster map with cloud cover confidence ranging from 0 for high confidence of clear sky to 100 for high confidence of cloudy sky [54]. This information was used to isolate pixels with a cloud probability above zero. Out of 34 images, 14 had at least one pixel covered by clouds. Table 2 below gives an overview. The study crop field covered 2006 pixels at 10 m GSD. All pixels with cloud probability above zero were masked and thus not considered for further processing. Masking removed these pixels from further processing.

Table 2. Number of pixels covered by clouds in each image and cloudy sky confidence (%) of removed pixels.

Image Date	N. Pixels *	Cloudy Sky Confidence		
		Min	Mean	Max
18 June 2016	6	1	1.83	2
18 July 2016	4	1	1.00	1
28 July 2016	4	1	1.00	1
24 August 2016	4	1	1.00	1
31 May 2017	70	1	1.17	3
3 June 2017	690	1	1.08	5
13 June2017	619	1	1.05	5
23 June 2017	4	2	2.00	2
10 July 2017	4	1	1.00	1
13 July 2017	4	4	4.00	4
2 August 2017	12	1	1.00	1
4 August 2017	4	1	1.00	1
12 August 2017	4	1	1.00	1
10 June 2018	4	3	3.00	3

* Number of pixels with cloudy sky confidence above zero. There are a total n. of 2006 pixels (10 m GSD) in the study area.

2.4. Vegetation Indices

Nine different vegetation indices (NDVI, NDRE1, NDRE2, GNDVI, GARVI, EVI, WDRVI, mWDRVI, and GCVI) were derived from Sentinel-2 images after resampling all bands to 10 m pixel size using SNAP software (Sentinel application platform) version 5.0. These indices are the most common VIs used for crop yield monitoring in the literature and were derived using Equations (1)–(9).

$$NDVI = \frac{\text{NIR} - \text{B4}}{\text{NIR} + \text{B4}}, \tag{1}$$

$$NDRE1 = \frac{\text{NIR} - \text{B5}}{\text{NIR} + \text{B5}}, \tag{2}$$

$$NDRE2 = \frac{\text{NIR} - \text{B6}}{\text{NIR} + \text{B6}}, \tag{3}$$

$$GNDVI = \frac{\text{NIR} - \text{B3}}{\text{NIR} + \text{B3}}, \tag{4}$$

$$GARVI = \frac{\text{NIR} - (\text{B3} - \text{B1} - \text{B5})}{\text{NIR} - (\text{B3} + \text{B1} - \text{B5})}, \tag{5}$$

$$EVI = \frac{\text{NIR} - \text{B4}}{\text{NIR} + 6\text{B4} - 7.5\text{B1} + 1} \times 2.5, \tag{6}$$

$$WDRVI = \frac{\alpha \times \text{NIR} - \text{B4}}{\alpha \times \text{NIR} + \text{B4}}, \tag{7}$$

$$mWDRVI = \begin{cases} NDVI & NDVI \leq 0.6 \\ WDRVI & NDVI > 0.6 \end{cases}, \tag{8}$$

$$GCVI = \left(\frac{NIR}{B3}\right) - 1, \tag{9}$$

where NDVI is the Normalized Difference Vegetation Index (Equation (1)), NDRE 1 and 2 are the Normalized Difference Red Edge calculated based on band numbers 5 and 6, respectively (Equations (2) and (3)), GARVI is the Green Atmospherically Resistant Vegetation Index (Equation (4)), GNDVI is the Green Normalized Difference Vegetation Index (Equation (5)), EVI is the Enhanced Vegetation Index (Equation (6)), WDRVI is the Wide Dynamic Range Vegetation Index (Equation (7)), and mWDRVI is a mixed WDRVI where the WDRVI value is used conditionally if the NDVI value is above 0.6, otherwise NDVI is used, as per the literature in [34,55] (Equation (8)). GCVI is the Green Chlorophyll Vegetation Index (Equation (9)). B1 is the reflectance of the blue band (432–453 nm), B3 is the reflectance of the green band (542–578 nm), B4 is the reflectance of the red band (649–680 nm), B5 and B6 are the reflectance of the vegetation red edge band at (697–712 nm) and (733–748 nm), respectively, and NIR is the reflectance of the near-infrared bands of the Sentinel-2 satellite images. For NIR, we tested bands 8, 8A, and 9, at (780–886 nm), (854–875 nm), and (935–955 nm), respectively, for all the VIs. The α value in WDRVI is a weighting factor equals to 0.15 as average value between 0.1 and 0.2 as it is reasonable according to literature [55]. The derived vegetation indices were analyzed and compared with the actual yield maps for each season. The correlation measured using R^2 value was calculated for each index at different crop ages.

2.5. Yield Prediction with Machine Learning

The prediction of a continuous variable, i.e., regression, can be done with several ML approaches. Three algorithms were tested in this investigation: multiple regression (MR), random forests (RF), and support vector machines (SVM). The last two are nonparametric methods, as the number of parameters in the model is not fixed, but changes depend on the data used for training—which usually grows as the training data volume increases [46]. These models were chosen because in the existing literature, they have been proven to yield better results when compared with other methods [56–60]. The independent variables were the reflectance values of the considered bands and the dependent variable to be predicted was the yield value. At each image, band values were used as independent variables to train a model using the values in the raster derived from the measured yield, as described in Section 2.2.

Multiple regression uses multiple simple linear regressions on the input variables using least squares optimization to define the best fit for each dependent variable as a function of the independent variable (measured yield). This is the simplest model and assumes a linear relationship between the yield and the band reflectance values, and that band values are not correlated. This last assumption is known to be untrue, as band values are correlated; thus, this method was applied to the first four principal components which contained 92% of variance.

Random Forests (RF) is a method based on decision trees for classification and regression. The training data are used to define decision boundaries that create the "trees" in the "forest" via split nodes in the decision tree process. The best combinations of splits are defined by a bootstrap approach. The available training data is sampled without replacement, keeping the remaining data for determining residuals from an independent set (out-of-bag validation) and thus comparing the accuracy metrics between combinations and choosing the best. Two main parameters need to be defined by the user: the number of features randomly sampled as candidates at each split—usually the square root of the total number of features—and the number of trees to grow.

The Support Vector Machine (SVM) method defines boundaries in high-dimensional space, i.e., a hyperplane, that separates training data into labelled classes, which, in our case, is a continuous variable (yield) for the regression task. Nonlinear boundaries use a nonlinear kernel function, in our

case, the Radial Basis kernel "Gaussian" RBF. For more information on the method, there is extensive literature on SVM applied to remote sensing [45,48,56,57].

In order to validate the tested models, the predicted yield was compared against the measured yield from independent samples. Only cells that were free from clouds were used by masking any cell with a cloud coverage probability above zero (see Table 2). The cause for using this conservative threshold is to avoid the noise from clouds taking into consideration that this study investigated the within-field variability of a relatively small area cultivated with the same crop through limited satellite spectral reflectance bands. Therefore, for each cloud-free date, we made 2006 observations with 12 variables, i.e., reflectance values of the land cover at the time the satellite image was recorded. In case of clouds, fewer cells were used.

The model was run 60 times, each time randomly dividing data into two parts and using one half for training and the remaining half for validation. This procedure was repeated to assess variation in accuracy metrics when using different point samples for training. Five accuracy metrics were extracted in order to obtain a thorough overview of the distribution of errors as per Equations (10)–(14).

$$ME = \frac{\sum_{i=1}^{n} y_i - x_i}{n}, \tag{10}$$

$$MAE = \frac{\sum_{i=1}^{n} |y_i - x_i|}{n}, \tag{11}$$

$$MAPE = \frac{\sum_{i=1}^{n} \left| \frac{y_i - x_i}{y_i} \right| \times 100}{n}, \tag{12}$$

$$RMSE = \sqrt{\frac{\sum_{i=1}^{n} (y_i - x_i)^2}{n}}, \tag{13}$$

$$R^2 = 1 - \frac{\sum_{i=1}^{n} (y_i - x_i)^2}{\sum_{i=1}^{n} (y_i - \overline{y})^2}, \tag{14}$$

where *MAE* is the mean absolute errors, *MAPE* is the mean absolute percentage error, *ME* is the mean error, R^2 is the *R*-squared, *RMSE* is the root mean square of errors, x is the measured yield value, y is the predicted yield value, n is the number of observations, i is the iteration of observations, and $\overline{y}$ is the mean value of predicted yield. All procedures were carried out in *R* with an rminer package [61,62]. The results show that random forests [63] provided the most accurate results. Therefore, random forests was used for further tuning and analysis (see Results section).

3. Results

The following sections report on results from VIs and machine learning approaches. Correlations of VIs with yield were analyzed to assess how VIs can potentially be used to model yield. The three machine learning models were assessed with the five mentioned accuracy metrics.

3.1. Vegetation Indices

Each year presented a different pattern of yield spatial distribution due to different soil characteristics, variable rate nitrogen application by the farmer, and other weather conditions. In general, the yield maps showed a high yield at the north-western zone of the field compared with the south-eastern zone in 2016 and 2017 (Figure 2). In 2018, yield improved in the south-eastern zone while yield decreased in the north-western zone compared to previous seasons.

Nine vegetation indices (NDVI, NDRE1, NDRE2, GNDVI, GARVI, EVI, WDRVI, mWDRVI, and GCVI) derived from each Sentinel-2 image calculated with three different NIR bands (8, 8A, and 9) were correlated with the actual yield map of each year. In general, correlations based on bands 8 and 8A were higher than those based on band 9. Band 8 and 8A correlations had the same trend for all

seasons and at all crop ages with slight differences. Band 9 has a spatial resolution of 60 m which provided only 57 pixels for the whole study field compared to band 8A and 8, which have a spatial resolution of 20 and 10 m and provided 516 and 2067 pixels, respectively. The higher spatial resolution could describe the field variability more accurately and improve the correlation results. Therefore, VIs based on band 8 were considered for further analysis.

The correlation between vegetation indices and corn grain yield (Figure 3) were low at the vegetative growth stages and early reproductive development stages (first 80 days of crop age) for 2017 and 2018 seasons. This correlation increased during the grain filling stage R3 (90 to 110 days) and reached its peak at the physiological maturity stage R4–R6 (105 to 135 days). This trend could be realized from the three seasons correlations (R^2 value), as shown in Figure 3. In 2016, the coefficient of determination (R^2 value) started from less than 0.2 at a crop age of 80 days (R3) and reached the highest R^2 value of 0.48 at 137 days (R6) from GNDVI. In 2017, a clearer trend was observed due to the higher number of available images, starting from an R^2 value of less than 0.2 at a crop age of 70 days (R2) and more than 0.35 for five different images from a crop age of 110 to 135 days (R4–R6). The highest R^2 value was for GNDVI compared to the other investigated indices at all stages, which reached a peak of 0.42 at the R6 stage at a crop age of 135 days. In 2018, R^2 values were not stable due to fog and blur in the images that affected the image quality but followed the same trend as previous seasons. The R^2 values started from less than 0.1 at a crop age between 60 and 100 days (R1–R4), then improved to reach the peak of 0.37 from GARVI and 0.36 from GNDVI at a crop age of 130 days (R6). All correlations between VIs and corn grain yield for all satellite image dates are available in the Supplementary files.
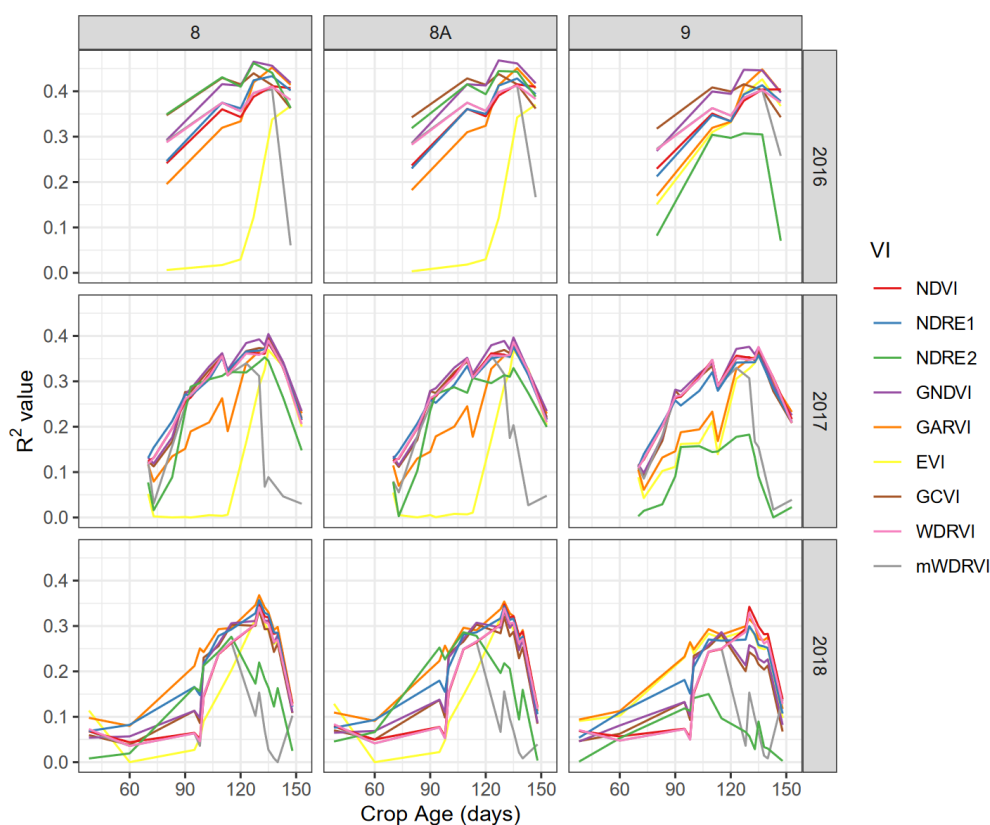
Figure 3. Coefficient of determination (R^2 value) between vegetation indices and actual yield at different crop ages for the three seasons. The three columns represent different NIR bands used.

GARVI provided the highest correlations in 2018 slightly higher than GNDVI. GARVI is more resistant to atmospheric effects, as described by Gitelson et al. [30], which explain GARVI's trend for this season in particular. Moreover, the correlation decreased dramatically at a crop age of 140 days

for the 2017 and 2018 seasons with a R^2 value of less than 0.25, while it decreased to 0.4 for 2016. After 140 days, the crop enters the stage of full maturity and leaves turns from green to brown, thus decreasing the coefficient of determination R^2 value. The highest R^2 value was observed from GNDVI at crop ages of 127, 135, and 130 days for 2016, 2017, and 2018, respectively. The corn yield maps after kriging and resampling to a 10 m pixel size with mostly correlated GNDVI and corresponding R^2 graph are shown in Figure 4. In Figure 4, GNDVI and yield maps are shown with the same color map stretched with the histogram equalization method.
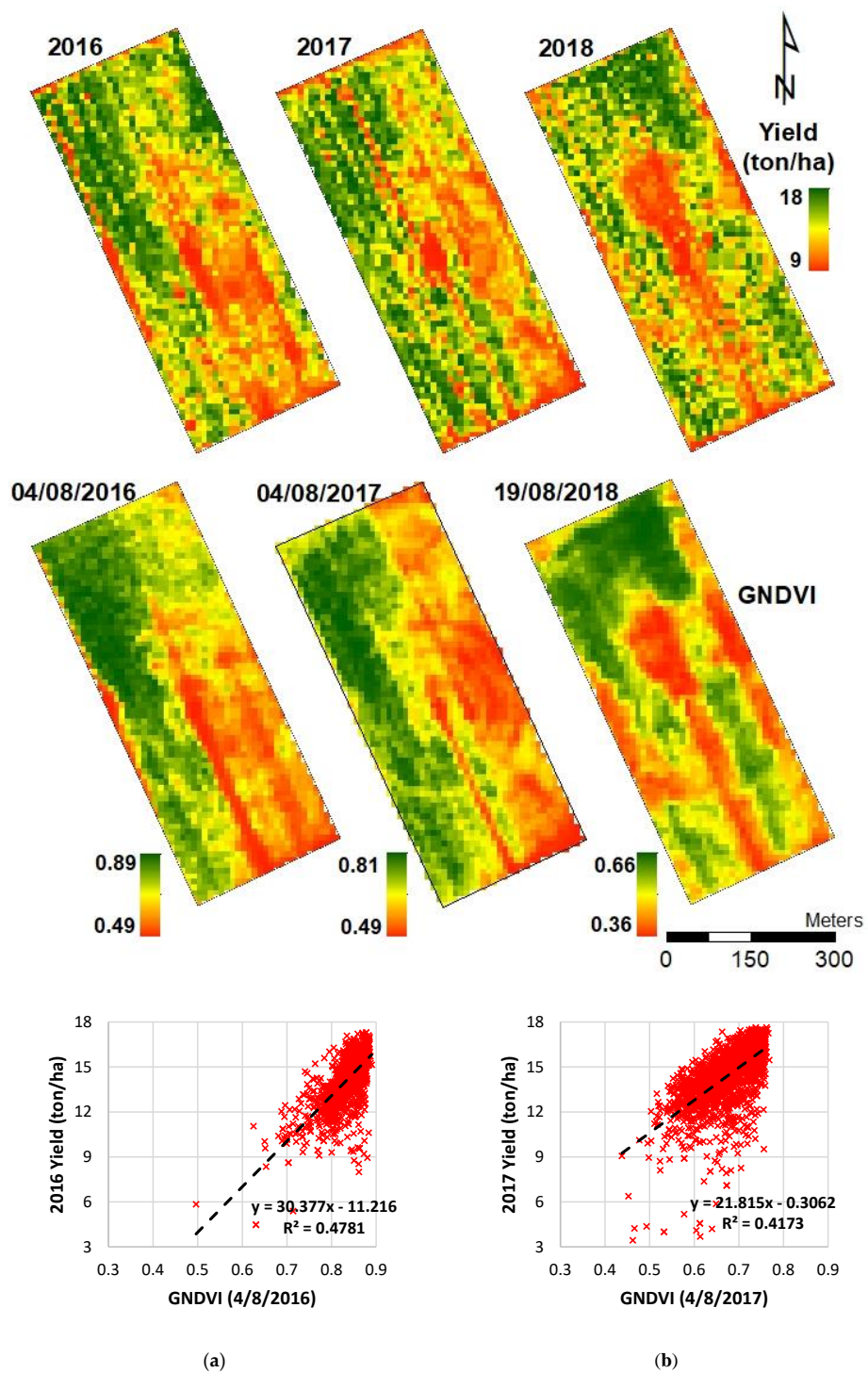
Figure 4. *Cont.*
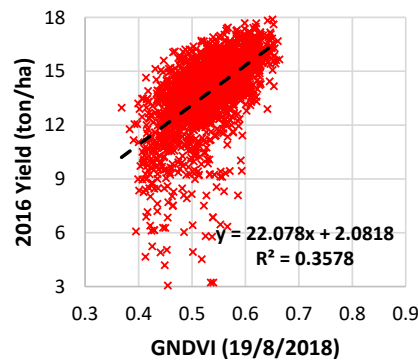
(**c**)

Figure 4. Measured yield maps (top) and Green Normalized Difference Vegetation Index (GNDVI) maps of date with a higher coefficient of determination for each year (middle) and corresponding scatter plot, equations, coefficient R^2 values where p values < 0.001 (bottom (**a**) for 2016, (**b**) for 2017 and (**c**) for 2018 season).

3.2. Machine Learning Models

The random forests algorithm can be tuned by changing two parameters: the number of trees (Nt) and the number of features (Nf). Iterative methods to find the best Nt and Nf combinations were applied by testing 3 × 5 combinations of Nf ∈ {4, 8, 12} and Nt ∈ {50, 100, 120, 200, 500}. The best combination resulted in Nf = 4 and Nt = 120. Each node in a tree is split by randomly selecting Nf features from the d-dimensional input feature space. Figure 5 shows how accuracy grows by increasing the number of trees, with the optimal value when no significant increase is seen. Figures 6 and 7 show that the results were optimal at a certain time from planting the crops, which is in line with results from vegetation indices correlations but with a higher overall R^2 value.
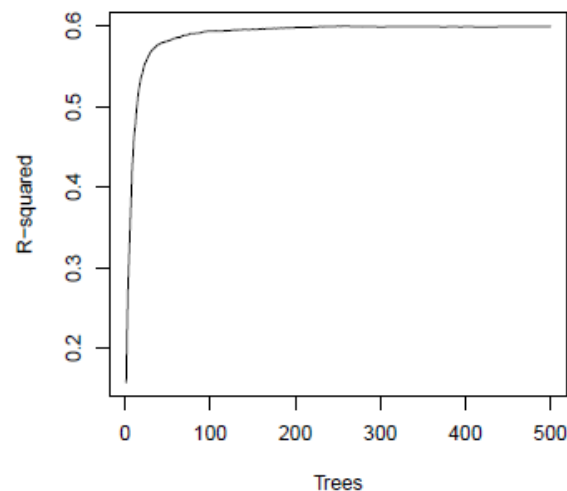
Figure 5. Improvement of fit versus the number of trees used in the Random Forests method.

The Random Forests method gave more accurate results when compared with other types of models that use decision trees and neural network ensembles (Figure 6). For each training and validation step, more runs were carried out, as mentioned in the Methods section; therefore, variance can be reported and is visible in the plot as standard deviation whiskers (Figure 6). Only ME had a high enough value of standard deviation to be visible in the plot, showing that the absolute accuracy metrics are significantly different between methods. This is coherent with the existing literature [56,57].

Figure 6 shows the result of the five calculated accuracy metrics, as reported in Equations (10)–(14). The mean absolute error (MAE) and the same as a percentage (MAPE) can distinguish how the best ML method ranges between 0.7 and 1.0 ton/ha, which corresponds to 5–8% of measured yields. Mean error is useful to assess bias; support vector machines ME values show that predicted yield values underestimated with respect to measured values. The whiskers in Figure 6 in the plot of the mean error show the variation of bias of each model when predictions were compared with measured yield values. This variation is +/− 0.05 ton/ha, which is minimal considering the 9 to 18 ton/ha range within-field zones. The correlation coefficient is reported for comparison reasons against the correlations found using the VIs reported in the previous section. Root mean square of errors is an important metric that is more sensitive than MAE to residuals of predicted and measured yield values.

The results in Figure 7 report the accuracy of each model trained using certain images at certain dates (rows) when predicting yield values using other images from other dates (columns). More is discussed on this in the next section. The most accurate results (low MAE values) were provided by the 2016 images compared to 2017 and 2018. The availability of more images in 2017 and 2018 showed that MAE values are higher during the early and late corn growing stages which is in line with high correlations in R4–R6 growing stages.

Figure 6. Accuracy metrics (average and 1× standard deviation) of several machine learning methods: multiple regression (MR), random forests (RF), and support vector machines (SVM). Values are in kg for error metrics.

	2016-06-18	2016-07-18	2016-07-28	2016-08-04	2016-08-14	2016-08-24	2017-05-31	2017-06-03	2017-06-13	2017-06-20	2017-06-23	2017-07-03	2017-07-10	2017-07-13	2017-07-23	2017-07-30	2017-08-02	2017-08-04	2017-08-12	2017-08-22	2018-05-19	2018-06-10	2018-07-15	2018-07-18	2018-07-20	2018-07-28	2018-08-04	2018-08-17	2018-08-19	2018-08-22	2018-08-24	2018-08-27	2018-08-29	2018-09-06
fit2016-06-18	256	973	993	915	1160	2576	3049	3966	2720	1454	1355	1303	1415	1758	1510	1298	2638	2529	3589	3554	3004	1452	1363	1531	1379	1498	1399	3305	3125	3213	3163	3251	3100	3251
fit2016-07-18	959	242	728	809	1235	2866	5248	3459	3725	2180	1419	1481	2010	3016	2546	3273	3829	4032	3370	4906	4743	1858	2442	1801	1626	1915	3126	3224	4258	4151	4330	4041	4352	4045
fit2016-07-28	907	689	242	766	977	2774	4614	3492	3641	1836	1411	1458	1615	2864	2331	2966	3529	3823	3169	4563	4134	1651	2048	1643	1495	1830	2672	3219	4079	3968	4105	3890	4114	3814
fit2016-08-04	1017	866	940	244	1278	2161	4795	2764	2917	1510	1401	1362	1510	2512	1814	2911	2685	2958	2384	4415	4332	1470	1930	1597	1490	1699	2302	2315	3778	3619	3938	3391	3911	3412
fit2016-08-14	1052	935	945	856	240	1637	3840	1910	2126	1180	1180	1225	1078	2043	1361	1825	2266	2435	1876	3631	3474	1354	1352	1375	1249	1245	1361	1936	3284	3181	3086	2960	3135	2918
fit2016-08-24	1067	1047	1003	1052	1000	242	4727	1161	1360	1326	1293	1326	1419	1307	1259	1523	1301	1508	1013	3158	3154	1436	1305	1484	1346	1218	1222	1054	2713	2370	2845	2352	2850	2371
fit2017-05-31	1231	1138	1123	1112	1107	1173	375	1175	1114	1348	1381	1397	1402	1381	1403	1344	1355	1373	1335	1216	2376	1577	1510	1642	1531	1552	1537	1571	1567	1588	1566	1615	1561	1626
fit2017-06-03	1278	1274	1251	1070	843	757	6876	358	1460	1275	1383	1423	1253	1500	1286	1219	1117	1332	983	4381	5705	1650	1271	1673	1515	1497	1060	1234	3811	2023	5267	2065	4226	1844
fit2017-06-13	1158	1175	1151	1036	952	901	6635	1681	344	1304	1390	1369	1356	1258	1245	1109	1033	1127	1533	4992	6443	1615	1431	1647	1455	1557	1361	1415	4441	3543	5468	3467	4617	3081
fit2017-06-20	2764	1808	2144	1058	991	3753	7353	4395	4652	346	3013	3111	1238	4641	3201	3070	4564	5534	4381	7140	6814	2563	1637	2371	1606	1824	2778	4652	6658	6497	6519	6217	6603	6345
fit2017-06-23	1082	1172	1110	813	784	4483	6813	5791	5404	1668	346	1186	1674	3874	2887	2839	5287	5467	5525	6750	6067	1609	2026	1925	1638	1765	2653	5355	6151	6339	6147	6378	6175	6219
fit2017-07-03	1065	1328	1297	853	908	4265	7842	4990	5650	1225	1090	347	1398	5029	2625	3307	5787	6452	5069	7797	7243	1556	1913	1674	1252	1675	3311	5867	7426	7295	7293	7170	7298	7088
fit2017-07-10	900	862	850	1157	889	3044	7921	3463	3987	1015	1123	1138	340	3656	1754	2787	3999	4511	3577	7199	7357	1328	1705	1420	1371	1491	2426	3907	6137	5845	7067	6054	6948	5779
fit2017-07-13	849	1150	1056	973	906	2089	7208	2408	2017	1274	1210	1153	1175	347	1063	1147	2478	2422	2505	5812	6749	1483	1402	1488	1375	1398	1295	2206	4896	4165	5397	4207	5655	3593
fit2017-07-23	1087	1258	1217	842	797	2725	8080	3510	2938	1103	1274	1230	1093	2441	336	2143	3135	3811	3527	7443	7319	1642	2092	1347	1281	1172	1566	3969	6972	6590	7076	6396	7093	6481
fit2017-07-30	831	1205	1220	1379	1012	1459	6578	2359	2554	1376	1064	1070	1042	2189	1445	339	2035	2115	1905	4129	6714	1451	1374	1584	1738	1593	1448	2280	2432	2236	3114	2222	3480	2023
fit2017-08-02	1172	1082	1174	1003	998	971	7300	1619	1112	1222	1284	1331	1289	1264	1347	1190	336	1105	1379	4588	7065	1532	1289	1416	1431	1329	1184	1455	2530	2121	3864	2464	4255	2196
fit2017-08-04	1361	1302	1299	1275	1097	932	5973	1442	1137	1426	1458	1449	1437	1150	1343	1012	1090	342	1253	4788	7084	1761	1493	1908	1903	1915	1258	1283	2990	1957	4070	2283	3950	1893
fit2017-08-12	1208	1226	1232	861	805	913	6163	1296	2306	1179	1401	1416	1231	2092	1172	2544	1720	2749	329	5619	6521	1690	1772	1404	1175	1061	1910	1415	3959	3481	5639	3565	5626	3041
fit2017-08-22	1017	1005	1009	1026	1021	1437	7586	1187	1433	1320	1305	1344	1284	1816	1360	1210	1514	1568	1436	343	3309	1355	1349	1347	1384	1381	1369	1692	1601	1205	1374	1052	1183	1083
fit2018-05-19	3855	3853	3853	3852	3852	3656	6000	3242	4485	4098	4094	4071	4094	4032	4052	4097	3913	3809	2791	2244	403	3619	3620	3549	3620	3618	3620	2465	2743	2043	2369	1657	1875	1398
fit2018-06-10	1279	1178	1141	2142	2981	2773	7588	3615	3860	3343	1533	1590	2641	3514	1558	5810	3850	4624	3322	6873	6594	404	4266	1464	2754	2714	4753	3501	6388	6010	6566	5957	6501	5615
fit2018-07-15	1389	1175	1143	742	1340	1501	4957	1249	1870	1393	1505	1535	1436	2332	1241	2671	2094	2355	1267	4361	4405	1630	393	1829	1325	1265	1873	1848	4177	3394	4318	3359	3940	3258
fit2018-07-18	1140	909	1094	2833	4214	4181	6420	3434	4374	3389	1474	1281	3491	3253	2262	5611	4622	4532	3413	4974	4558	1714	4541	390	2767	2910	5150	3233	4559	4519	4565	4246	4566	4169
fit2018-07-20	1231	1170	1112	816	1717	2147	3969	3677	4389	1590	1284	1460	1232	3966	1344	3875	3160	3710	2779	3834	3447	1443	3345	1354	396	1492	3255	3473	3501	3473	3288	3453	3291	3531
fit2018-07-28	1357	1159	1075	922	1646	2632	6903	2812	3334	1538	1318	1460	1280	2898	1056	4686	3887	4697	2602	6618	6168	1507	3153	1459	1218	375	3238	3617	6105	6048	6213	5940	6183	5979
fit2018-08-04	1710	1635	1660	1201	1120	1208	6193	1852	2229	1445	1724	1665	1530	2311	1109	2097	1761	2402	1433	5583	5658	2086	1193	1879	1725	1734	372	2179	4756	4318	5194	4155	5199	4035
fit2018-08-17	1513	1454	1407	924	1056	1848	7557	1370	1409	1304	1481	1527	1299	1227	1426	3195	2461	3141	1168	6274	6279	1820	1298	1930	1290	1514	1280	371	6158	4741	6228	4225	5986	4018
fit2018-08-19	1987	1998	1995	1973	1839	1458	6480	1163	1410	1884	1892	1919	1862	1612	1916	1394	1425	1413	1016	2653	5470	2402	2402	2427	2386	2416	2238	1282	378	1353	2167	2022	2622	2436
fit2018-08-22	1783	1793	1786	1708	1602	1359	6944	1176	1077	1699	1727	1763	1669	1310	1739	1282	1326	1344	1081	3037	5434	2198	1889	2219	2120	2165	2012	1391	1917	383	3303	1597	2430	3102
fit2018-08-24	1865	1877	1876	1874	1813	1822	5051	1284	1333	1811	1805	1833	1793	1312	1841	1578	1744	1679	1078	1621	4259	2285	2291	2308	2282	2297	2173	1487	1098	1090	381	1465	1417	2221
fit2018-08-27	1640	1644	1637	1150	1476	1293	6302	1049	1138	1567	1622	1657	1533	1325	1543	1008	1249	1038	1314	3015	5106	2052	1358	1927	1939	1981	1717	1549	1595	1215	3012	385	2118	1721
fit2018-08-29	2183	2199	2198	2189	2142	2043	5613	1366	1152	2068	2055	2079	2040	1358	2077	1870	1939	1869	1296	2063	5692	2600	2556	2615	2606	2614	2546	1763	1124	1197	1163	1094	389	1453
fit2018-09-06	1196	1173	1166	1034	965	760	6518	1075	1534	1304	1349	1376	1293	1948	1360	1231	1055	1143	1389	5048	5943	1580	1266	1597	1507	1522	1250	1563	3371	2524	5501	2048	5141	379

Figure 7. Mean absolute error (MAE) values from the Random Forests model that was trained with Sentinel-2 data on a certain date (rows) applied for prediction using Sentinel-2 images at all dates (columns). Table color scaling from green for low values to red for high values. Values are in kg for error metrics.

4. Discussion

The first outcome of this study is that GNDVI showed the highest correlation between VI and corn grain yield. This result is in line with Shanahan et al. [41], who reported the same index from aircraft imagery at a small scale. In addition, Schwalbert et al. [19] and Peralta et al. [18] reported that GNDVI and NDVI reflected the potential on corn yield prediction models. The difference between the examined VIs was not large, except for EVI, but GNDVI showed a clearer trend and the highest correlations. This result is clearer in the 2017 season, while other seasons have more fluctuation in other VIs and less image availability. Gitelson et al. [30] reported that GNDVI is more sensitive to the chlorophyll concentration in a wide range of chlorophyll variations. Additionally, they reported that the reflectance range between 520 and 630 nm is the most sensitive for chlorophyll. This range matches with the green band B3 of Sentinel-2 data that ranges between 524 and 596 nm. Meanwhile, Tan et al. [64] reported that GNDVI was the most positively correlated vegetation index with FPAR for corn canopies which subsequently describes the strong relation to corn biomass and yield.

Secondly, GNDVI derived from Sentinel-2 images in the study field could provide a clear description of the corn grain yield spatial variability within-field scale for around 1 month between the end of grain filling and physiological maturity stages. This period is around the physiological maturity stages (R4–R6) at crop ages of 105 to 135 days from planting and mostly between mid-July and mid-August in North Italy. This period was mentioned by Ferencz et al. [42] in a Hungarian county scale, Shanahan et al. [41], and Maestrini and Basso [40] in the USA for corn yield prediction. The consistency for this period in the USA, Hungary, and Italy and with multiple scales supports defining it as the most suitable corn yield prediction time. This period is the summer season with less probability of clouds and fog, and Sentinel-2 could provide about six images during this month, which could describe the corn grain yield variability within-field.

Machine learning provides overall higher R^2 and more robust results than the VIs approach. Practical results from this study are clearly the application of random forests after 105 days from planting, training the model with a few ground truths sampled over the field, and then applying the trained model over other fields that must be modelled. Evidently, fields must have similar characteristics. The final target is to have a mapped spatial distribution of corn yield over the field of interest that could support farmers for site specific applications.

Another result pertaining to the application of machine learning models with Sentinel-2 reflectance timeseries data for crop yield prediction is depicted in Figure 7. Figure 7 reports on the accuracy of a model that was fitted by training with imagery from a certain date (rows), applied to imagery from all other dates (columns). The diagonal row in this table represents fitting and modelling on the same image and, as expected, provided the best performance. Other combinations show how well a model that is fitted on one image date performs on another image date. Figure 7 shows that the model must be used in the same conditions of crop growing stage to replicate acceptable accuracies. Machine learning methods are nonparametric methods and have many advantages, as mentioned here and in other studies, but are not easily interpreted and, therefore, replication of a model with imagery from other dates or different conditions is not advised.

Another aspect worth discussing is that correlations became worse from 2016 to 2018 for VIs. In machine learning, it is clear that compared to other models, 2016 provided the highest coefficients of determination (Figures 6 and 7). In Figure 7, the 2016 images (columns) provided better accuracy values with other models (rows) than other years, in particular, in August, as the columns show lower MAE values. There are possible explanations for 2016 being a better year for predicting yield values that can be brought forward, even if at this stage, they are only hypotheses. One important point to consider is the accuracy of the measured yield values. The measured yield values are used as "truth", but as all measures go, they are prone to a certain degree of error. The method used for measuring provides about 10 times higher accuracy than prediction models, but it can record values incorrectly, such as explained in the materials section, i.e., border effects, harvester passing twice. Then, it might be possible that seasons 2017 and 2018 yield data underwent higher errors due to unpredicted or

unseen sensor or measurement distortions such as GPS and yield sensors' inaccuracies or calibration errors from year to year. This can explain the overall difference in correlation and prediction accuracy between years, as the measured yield is fixed per year. Burke and Lobell [35] have found R^2 up to 0.4 for corn yield prediction from RS data, stressing the importance of the quality of the field measures. Another possible and probably more realistic hypothesis can be related to atmospheric conditions, as the images in 2017 and 2018 might have suffered from more opaque atmospheric conditions, not so much to be detected as cloud probability by the sen2cor algorithm used in Sentinel-2 processing.

Even the relation between yield and VIs are affected by spatial and temporal constraints, as reported by many researchers [19], but it could be used for identifying management zones [7,65], evaluating within-field variability and subsequently, the need for PA practices. According to the study results, Sentinel-2 could assess only 40–60% of field variability: such percentage is clearly unsatisfactory if seen at single pixel level, but is fully acceptable in common PA practices, where management zones are to be defined. Indeed, in this case, a relatively high number of values are averaged within each MZ (typically larger than 1 acre, corresponding to at least 40 pixels) eventually allowing reduction of variability and a corresponding increase of overall robustness of the method. Within-field variability is common due to variations in soil type, topography, nutrient level, and many other factors of agricultural fields. Mapping this variability, delineating to homogeneous zones, and applying the variable rate application of agricultural inputs leads to more profitable and efficient management practices. In addition, the archived Sentinel-2 images could provide an important source for monitoring fields' history and the cumulative production for each zone. Recent studies reported that the profit of PA applications ranged between −30 $/ha and 70 $/ha and about 25% of studies reported economic losses [66]. In view of this, evaluating field spatial variability on previous seasons from archived satellite images could be a simple approach to evaluate the actual need for site-specific management practices. Mulla [67] highlighted the necessity of integrating archived satellite images for PA decision support systems and this approach could be a promising application in this field. Moreover, monitoring yield variability within fields through archived satellite images could be applied for different crops, varieties, countries, and farming management practices to widen the use of archived data.

5. Conclusions

A field study was conducted to investigate the possibility of monitoring corn grain yield within a 22-ha field using Sentinel-2 satellite images. Actual corn yield maps for three seasons were correlated with different vegetation indices and crop ages through the implementation of machine learning techniques. Monitoring the within-field variability of corn yield was possible and the R^2 value reached more than 0.5 in some cases. The main findings can be summarized as follows:

- GNDVI was the most correlated VI with corn grain yield at the field scale;
- the most suitable time for corn yield forecasting was during the physiological maturity stages (R4–R6) between 105 and 135 days from the planting date, i.e., between mid-July and mid-August;
- this period is not only the most correlated, but also is provides a higher number of satellite images due to reduced cloud events in the area considered;
- Random Forests was the most accurate machine learning technique in corn yield monitoring with R^2 values almost reaching 0.6 in an independent validation set;
- the Random Forests method works best when trained with imagery close to the above-mentioned most suitable time for forecasting; applying it to images at different crop stages is not advised.

The overall question "can Sentinel-2 imagery be used to predict corn yield values?" can be answered by saying that in a scenario with expected yields between 9 and 18 ton/ha, a likely prediction with a 10% error can be expected using a Random Forests model trained with a few ground samples taken between 105 and 135 days of crop age. Without ground samples of yield values, thus, with less effort on the ground, one can validly use GNDVI at the same crop age range for understanding the spatial variation of yield. Future research will use more tests to understand the ideal combination

of volume of training data and the spatial distribution of training data for understanding the best economical combination for an accurate prediction of corn yield with the least effort in terms of surveying training data for the model.

References

1. Ross, K.W.; Morris, D.K.; Johannsen, C.J. A Review of Intra-Field Yield Estimation from Yield Monitor Data. *Appl. Eng. Agric.* **2008**, *24*, 309–317. [CrossRef]

2. Trotter, T.F.; Fraizer, P.S.; Mark, G.T.; David, W.L. Objective Biomass Assessment Using an Active Plant Sensor (Crop circletm)—Preliminary Experiences on a Variety of Agricultural Landscapes. In Proceedings of the 9th International Conference on Precision Agriculture (ICPA), Denver, CO, USA, 20–23 July 2008.

3. Pezzuolo, A.; Basso, B.; Marinello, F.; Sartori, L. Using SALUS model for medium and long term simulations of energy efficiency in different tillage systems. *Appl. Math. Sci.* **2014**, *8*, 6433–6445. [CrossRef]

4. Al-Gaadi, K.A.; Hassaballa, A.A.; Tola, E.; Kayad, A.; Madugundu, R.; Assiri, F.; Alblewi, B. Characterization of the spatial variability of surface topography and moisture content and its influence on potato crop yield. *Int. J. Remote Sens.* **2018**, *39*, 8572–8590. [CrossRef]

5. Lobell, D.B.; Thau, D.; Seifert, C.; Engle, E.; Little, B. A scalable satellite-based crop yield mapper. *Remote Sens. Environ.* **2015**, *164*, 324–333. [CrossRef]

6. Kross, A.; McNairn, H.; Lapen, D.; Sunohara, M.; Champagne, C. Assessment of RapidEye vegetation indices for estimation of leaf area index and biomass in corn and soybean crops. *Int. J. Appl. Earth Obs. Geoinf.* **2015**, *34*, 235–248. [CrossRef]

7. Blackmore, S. The Role of Yield Maps in Precision Farming. Ph.D. Thesis, Cranfiled University at Silsoe, Cranfiled, UK, 2003.

8. Bouman, B.M. Crop modelling and remote sensing for yield prediction. *Neth. J. Agric. Sci.* **1995**, *43*, 143–161.

9. Yao, F.; Tang, Y.; Wang, P.; Zhang, J. Estimation of maize yield by using a process-based model and remote sensing data in the Northeast China Plain. *Phys. Chem. Earth* **2015**, *87–88*, 142–152. [CrossRef]

10. Huang, Y.; Zhu, Y.; Li, W.; Cao, W.; Tian, Y. Assimilating Remotely Sensed Information with the WheatGrow Model Based on the Ensemble Square Root Filter forImproving Regional Wheat Yield Forecasts. *Plant Prod. Sci.* **2013**, *16*, 352–364. [CrossRef]

11. Morel, J.; Todoroff, P.; Bégué, A.; Bury, A.; Martiné, J.F.; Petit, M. Toward a satellite-based system of sugarcane yield estimation and forecasting in smallholder farming conditions: A case study on reunion island. *Remote Sens.* **2014**, *6*, 6620–6635. [CrossRef]

12. Bala, S.K.; Islam, A.S. Correlation between potato yield and MODIS-derived vegetation indices. *Int. J. Remote Sens.* **2009**, *30*, 2491–2507. [CrossRef]

13. Mkhabela, M.S.; Bullock, P.; Raj, S.; Wang, S.; Yang, Y. Crop yield forecasting on the Canadian Prairies using MODIS NDVI data. *Agric. For. Meteorol.* **2011**, *151*, 385–393. [CrossRef]

14. Gao, F.; Anderson, M.; Daughtry, C.; Johnson, D. Assessing the variability of corn and soybean yields in central Iowa using high spatiotemporal resolution multi-satellite imagery. *Remote Sens.* **2018**, *10*, 1489. [CrossRef]

15. Lobell, D.B.; Ortiz-Monasterio, J.I.; Asner, G.P.; Naylor, R.L.; Falcon, W.P. Combining field surveys, remote sensing, and regression trees to understand yield variations in an irrigated wheat landscape. *Agron. J.* **2005**, *97*, 241–249.

16. Kayad, A.G.; Al-Gaadi, K.A.; Tola, E.; Madugundu, R.; Zeyada, A.M.; Kalaitzidis, C. Assessing the spatial variability of alfalfa yield using satellite imagery and ground-based data. *PLoS ONE* **2016**, *11*, e0157166. [CrossRef]

17. Al-Gaadi, K.A.; Hassaballa, A.A.; Tola, E.; Kayad, A.; Madugundu, R.; Alblewi, B.; Assiri, F. Prediction of potato crop yield using precision agriculture techniques. *PLoS ONE* **2016**, *11*, e0162219. [CrossRef]

18. Peralta, N.R.; Assefa, Y.; Du, J.; Barden, C.J.; Ciampitti, I.A. Mid-season high-resolution satellite imagery for forecasting site-specific corn yield. *Remote Sens.* **2016**, *8*, 848. [CrossRef]

19. Schwalbert, R.A.; Amado, T.J.C.; Nieto, L.; Varela, S.; Corassa, G.M.; Horbe, T.A.N.; Rice, C.W.; Peralta, N.R.; Ciampitti, I.A. Forecasting maize yield at field scale based on high-resolution satellite imagery. *Biosyst. Eng.* **2018**, *171*, 179–192. [CrossRef]

20. Asrar, G.; Kanemasu, E.T.; Yoshida, M. Estimates of leaf area index from spectral reflectance of wheat under different cultural practices and solar angle. *Remote Sens. Environ.* **1985**, *17*, 1–11. [CrossRef]

21. Patel, N.K.; Patnaik, C.; Dutta, S.; Shekh, A.M.; Dave, A.J. Study of crop growth parameters using Airborne Imaging Spectrometer data. *Int. J. Remote Sens.* **2001**, *22*, 2401–2411. [CrossRef]

22. Tucker, C.J.; Holben, B.N.; Elgin, J.H.; McMurtrey, J.E. Remote sensing of total dry-matter accumulation in winter wheat. *Remote Sens. Environ.* **1981**, *11*, 171–189. [CrossRef]

23. Ferencz, C.; Bognár, P.; Lichtenberger, J.; Hamar, D.; Tarcsai, G.; Timár, G.; Molnár, G.; Pásztor, S.; Steinbach, P.; Székely, B.; et al. Crop yield estimation by satellite remote sensing. *Int. J. Remote Sens.* **2004**, *25*, 4113–4149. [CrossRef]

24. Sibley, A.M.; Grassini, P.; Thomas, N.E.; Cassman, K.G.; Lobell, D.B. Testing remote sensing approaches for assessing yield variability among maize fields. *Agron. J.* **2014**, *106*, 24–32. [CrossRef]

25. Dubbini, M.; Pezzuolo, A.; De Giglio, M.; Gattelli, M.; Curzio, L.; Covi, D.; Yezekyan, T.; Marinello, F. Last generation instrument for agriculture multispectral data collection. *Agric. Eng. Int. CIGR J.* **2017**, *19*, 87–93.

26. Báez-González, A.D.; Chen, P.; Tiscareño-López, M.; Srinivasan, R. Using Satellite and Field Data with Crop Growth Modeling to Monitor and Estimate Corn Yield in Mexico. *Crop Sci.* **2002**, *42*, 1943–1949. [CrossRef]

27. Lobell, D.B. The use of satellite data for crop yield gap analysis. *Field Crop. Res.* **2013**, *143*, 56–64. [CrossRef]

28. Tucker, C.J. Red and photographic infrared linear combinations for monitoring vegetation. *Remote Sens. Environ.* **1979**, *8*, 127–150. [CrossRef]

29. Huete, A.R. A soil-adjusted vegetation index (SAVI). *Remote Sens. Environ.* **1988**, *25*, 295–309. [CrossRef]

30. Gitelson, A.A.; Kaufman, Y.J.; Merzlyak, M.N. Use of a green channel in remote sensing of global vegetation from EOS- MODIS. *Remote Sens. Environ.* **1996**, *58*, 289–298. [CrossRef]

31. Panda, S.S.; Ames, D.P.; Panigrahi, S. Application of vegetation indices for agricultural crop yield prediction using neural network techniques. *Remote Sens.* **2010**, *2*, 673–696. [CrossRef]

32. Xue, J.; Su, B. Significant Remote Sensing Vegetation Indices: A Review of Developments and Applications. *J. Sensors* **2017**, *2017*, 1–17. [CrossRef]

33. Sakamoto, T.; Gitelson, A.A.; Wardlow, B.D.; Verma, S.B.; Suyker, A.E. Estimating daily gross primary production of maize based only on MODIS WDRVI and shortwave radiation data. *Remote Sens. Environ.* **2011**, *115*, 3091–3101. [CrossRef]

34. Sakamoto, T.; Gitelson, A.A.; Arkebauer, T.J. MODIS-based corn grain yield estimation model incorporating crop phenology information. *Remote Sens. Environ.* **2013**, *131*, 215–231. [CrossRef]

35. Burke, M.; Lobell, D.B. Satellite-based assessment of yield variation and its determinants in smallholder African systems. *Proc. Natl. Acad. Sci. USA* **2017**, *114*, 2189–2194. [CrossRef] [PubMed]

36. Bu, H.; Sharma, L.K.; Denton, A.; Franzen, D.W. Comparison of satellite imagery and ground-based active optical sensors as yield predictors in sugar beet, spring wheat, corn, and sunflower. *Agron. J.* **2017**, *109*, 299–308. [CrossRef]

37. Liao, C.; Wang, J.; Dong, T.; Shang, J.; Liu, J.; Song, Y. Using spatio-temporal fusion of Landsat-8 and MODIS data to derive phenology, biomass and yield estimates for corn and soybean. *Sci. Total Environ.* **2019**, *650*, 1707–1721. [CrossRef]

38. Fieuzal, R.; Marais Sicre, C.; Baup, F. Estimation of corn yield using multi-temporal optical and radar satellite data and artificial neural networks. *Int. J. Appl. Earth Obs. Geoinf.* **2016**, *57*, 14–23. [CrossRef]

39. Rojas, O. Operational maize yield model development and validation based on remote sensing and agro-meteorological data in Kenya. *Int. J. Remote Sens.* **2007**, *28*, 3775–3793. [CrossRef]

40. Maestrini, B.; Basso, B. Predicting spatial patterns of within-field crop yield variability. *F. Crop. Res.* **2018**, *219*, 106–112. [CrossRef]

41. Shanahan, J.F.; Schepers, J.S.; Francis, D.D.; Varvel, G.E.; Wilhelm, W.W.; Tringe, J.M.; Schlemmer, M.R.; Major, D.J. Use of remote-sensing imagery to estimate corn grain yield. *Agron. J.* **2001**, *93*, 583–589. [CrossRef]

42. Bognár, P.; Ferencz, C.; Pásztor, S.Z.; Molnár, G.; Timár, G.; Hamar, D.; Lichtenberger, J.; Székely, B.; Steinbach, P.; Ferencz, O.E. Yield forecasting for wheat and corn in Hungary by satellite remote sensing. *Int. J. Remote Sens.* **2011**, *32*, 4759–4767. [CrossRef]

43. Rahman, M.M.; Robson, A.; Bristow, M. Exploring the potential of high resolution worldview-3 Imagery for estimating yield of mango. *Remote Sens.* **2018**, *10*, 1866. [CrossRef]

44. Mas, J.F.; Flores, J.J. The application of artificial neural networks to the analysis of remotely sensed data. *Int. J. Remote Sens.* **2008**, *29*, 617–663. [CrossRef]

45. Yuan, H.; Yang, G.; Li, C.; Wang, Y.; Liu, J.; Yu, H.; Feng, H.; Xu, B.; Zhao, X.; Yang, X. Retrieving soybean leaf area index from unmanned aerial vehicle hyperspectral remote sensing: Analysis of RF, ANN, and SVM regression models. *Remote Sens.* **2017**, *9*, 309. [CrossRef]

46. Russell, S.; Norvig, P. *Artificial Intelligence A Modern Approach*, 3rd ed.; Prentice Hall: Upper Saddle River, NJ, USA, 2010; ISBN 9780136042594.

47. Liakos, K.G.; Busato, P.; Moshou, D.; Pearson, S.; Bochtis, D. Machine learning in agriculture: A review. *Sensors* **2018**, *18*, 2674. [CrossRef] [PubMed]

48. Ali, I.; Greifeneder, F.; Stamenkovic, J.; Neumann, M.; Notarnicola, C. Review of machine learning approaches for biomass and soil moisture retrievals from remote sensing data. *Remote Sens.* **2015**, *7*, 16398–16421. [CrossRef]

49. Yue, J.; Feng, H.; Yang, G.; Li, Z. A comparison of regression techniques for estimation of above-ground winter wheat biomass using near-surface spectroscopy. *Remote Sens.* **2018**, *10*, 66. [CrossRef]

50. Karimi, Y.; Prasher, S.O.; Patel, R.M.; Kim, S.H. Application of support vector machine technology for weed and nitrogen stress detection in corn. *Comput. Electron. Agric.* **2006**, *51*, 99–109. [CrossRef]

51. Han, L.; Yang, G.; Dai, H.; Xu, B.; Yang, H.; Feng, H.; Li, Z.; Yang, X. Modeling maize above-ground biomass based on machine learning approaches using UAV remote-sensing data. *Plant Methods* **2019**, *15*, 1–19. [CrossRef]

52. EUROSTAT. European Statistics on Agriculture, Forestry and Fisheries. Available online: https://ec.europa. eu/eurostat/data/database (accessed on 5 April 2019).

53. Drusch, M.; Del Bello, U.; Carlier, S.; Colin, O.; Fernandez, V.; Gascon, F.; Hoersch, B.; Isola, C.; Laberinti, P.; Martimort, P.; et al. Sentinel-2: ESA's Optical High-Resolution Mission for GMES Operational Services. *Remote Sens. Environ.* **2012**, *120*, 25–36. [CrossRef]

54. Louis, J. *S2 MPC—L2A Product Definition* Document. Available online: https://sentinel.esa.int/documents/ 247904/685211/S2+L2A+Product+Definition+Document/2c0f6d5f-60b5-48de-bc0d-e0f45ca06304 (accessed on 1 December 2019).

55. Gitelson, A.A. Wide Dynamic Range Vegetation Index for Remote Quantification of Biophysical Characteristics of Vegetation. *J. Plant Physiol.* **2004**, *161*, 165–173. [CrossRef]

56. Pirotti, F.; Sunar, F.; Piragnolo, M. Benchmark of Machine Learning Methods for Classification of a Sentinel-2 Image. *ISPRS Int. Arch. Photogramm. Remote Sens. Spat. Inf. Sci.* **2016**, *XLI-B7*, 335–340. [CrossRef]

57. Piragnolo, M.; Masiero, A.; Pirotti, F. Open source R for applying machine learning to RPAS remote sensing images. *Open Geospat. Data Softw. Stand.* **2017**, *2*, 16. [CrossRef]

58. Kim, N.; Lee, Y.W. Machine learning approaches to corn yield estimation using satellite images and climate data: A case of Iowa State. *J. Korean Soc. Surv. Geod. Photogramm. Cartogr.* **2016**, *34*, 383–390. [CrossRef]

59. Jeong, J.H.; Resop, J.P.; Mueller, N.D.; Fleisher, D.H.; Yun, K.; Butler, E.E.; Timlin, D.J.; Shim, K.M.; Gerber, J.S.; Reddy, V.R.; et al. Random forests for global and regional crop yield predictions. *PLoS ONE* **2016**, *11*, e0156571. [CrossRef] [PubMed]

60. Hunt, M.L.; Blackburn, G.A.; Carrasco, L.; Redhead, J.W.; Rowland, C.S. High resolution wheat yield mapping using Sentinel-2. *Remote Sens. Environ.* **2019**, *233*, 111410. [CrossRef]

61. Cortez, P. Package 'rminer'. Available online: https://cran.r-project.org/web/packages/rminer/index.html (accessed on 1 December 2019).

62. Cortez, P. *Package 'Rminer'*; Teaching Report; Department of Information System, ALGORITMI Research Centre, Engineering School: Guimares, Portugal, 2016; p. 59.

63. Breiman, L. Random forests. *Mach. Learn.* **2001**, *45*, 5–32. [CrossRef]

64. Tan, C.; Samanta, A.; Jin, X.; Tong, L.; Ma, C.; Guo, W.; Knyazikhin, Y.; Myneni, R.B. Using hyperspectral vegetation indices to estimate the fraction of photosynthetically active radiation absorbed by corn canopies. *Int. J. Remote Sens.* **2013**, *34*, 8789–8802. [CrossRef]

65. Patil, V.C.; Al-Gaadi, K.A.; Madugundu, R.; Tola, E.K.H.M.; Marey, S.A.; Al-Omran, A.M.; Khosla, R.; Upadhyaya, S.K.; Mulla, D.J.; Al-Dosari, A. Delineation of management zones and response of spring wheat (Triticum aestivum) to irrigation and nutrient levels in Saudi Arabia. *Int. J. Agric. Biol.* **2014**, *16*, 104–110.

66. Colaço, A.F.; Bramley, R.G.V. Do crop sensors promote improved nitrogen management in grain crops? *Field Crop. Res.* **2018**, *218*, 126–140. [CrossRef]

67. Mulla, D.J. Twenty five years of remote sensing in precision agriculture: Key advances and remaining knowledge gaps. *Biosyst. Eng.* **2013**, *114*, 358–371. [CrossRef]